Indian Journal of Pure & Applied Physics
Vol. 60, May 2022, pp. 395-400

A Simple Analytical Model of a GaN MODFET to Study its DC and RF Performance

Prabir Kumar Shit[a], Radha Raman Pal[a] & Sutanu Dutta[b]*

[a]Department of Physics, Vidyasagar University, Paschim Medinipur, West Bengal, India

[b]Department of Electronics, Vidyasagar University, Paschim Medinipur, West Bengal, India

Received 24 February 2022; accepted 19 April 2022

This work presents a theoretical study of a GaN MODFET considering accurate velocity field relation of GaN for a wide range of electric field. The analytical expression of different DC parameters such as drain current, mutual conductance and drain conductance of the device has been derived and their variation over different field regions has been investigated. This work has also been extended to study the RF parameters like cut-off frequency and maximum operating frequency of the device. The threshold voltage of the device is also derived and studied in terms of the thickness of the doped AlGaN layer and mole fraction of AlGaN. The mathematical model presented here is calibrated with the experimentally available results reported earlier and a good agreement has been observed.

Keywords: GaN MODFET; Theoritical Modeling; DC Characteristics; RF Characteristics; Threshold Voltage

1 Introduction

The modulation doped field effect transistors (MODFETs) are getting increasingly important in high power and high frequency electronic applications in recent days. The MODFETs based on GaAs and AlGaAs hetero junction are very popular for high frequency and microwave applications. A number of works have been carried out earlier to study the performance of a MODFET based on GaAs devices[1-6]. But for high temperature and high power device application, the utility of the GaAs devices are limited. The modulation doped devices based on wide band gap compound semiconductors are free from such limitations. Particularly, GaN material from III-V group becomes very important in high power and high temperature electronic applications for its large band gap, high electron mobility, large saturation electron velocity and high thermal conductivity etc. Another advantage of GaN is its minimum lattice mismatch with AlGaN that helps it to form a good hetero-junction device. These unique features and material properties have enable GaN a promising material for high power hetero-structure electronics. The performance of GaN MODFETs are also studied extensively in near past by a number of workers[7-15]. Some researchers have developed current models for GaN MODFET considering various issues of contemporary interests[16-22]. In all such calculations, the previous workers have considered the conventional mobility model to study the performance of a MODFET based on GaN. In low drain field, the mobility of electrons in 2DEG region is constant. But, the electron mobility in GaN becomes field dependent in higher field and is different for different field regions. For very high electric field, the velocity of electrons finally saturates. In addition, n-type GaN also shows negative differential mobility (NDR) for a particular band of electric field. In order to precise estimation of the drain current of the device, an accurate velocity-field relation should be followed. In all the previous works carried out so far, different mobility relations of electrons in different field regions are not considered in current modeling.

In this work, we consider an accurate velocity field relation of electrons in GaN including NDR to calculate the drain current of the device. The variation of drain current along with other device DC parameters such as threshold voltage, drain conductance and mutual conductance are studied with drain field. The advantage of this model is that it includes the wide band of field regions. In addition, RF parameters such as the cut-off frequency and maximum operating frequency of the device is calculated and studied with drain field and other parameters of interest.

2 Velocity-Field relation of electrons in GaN

The N-type GaN semiconductors shows negative differential resistance (NDR) and velocity-field

Corresponding author: (Email: sutanu@mail.vidyasagar.ac.in)

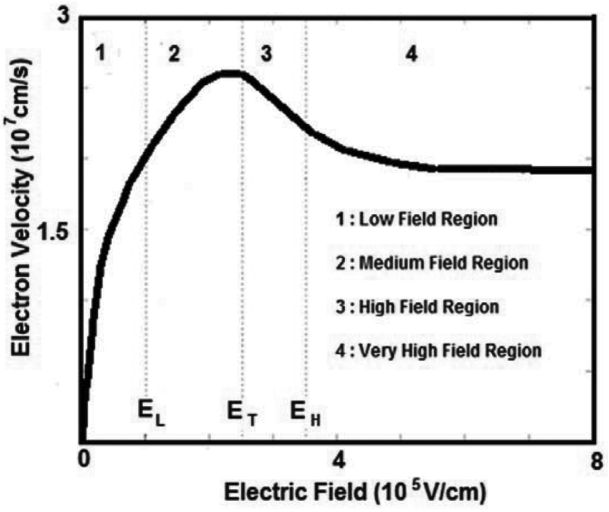

Fig. 1 — Electron Velocity *vs*. Field Characteristics of GaN[23]

Table 1 — Material and Device parameters used in calculations

Parameters	Value
α_1	2.7×10^{-4}cm^3/V^{2}s
α_2	130cm^2/*Vs*
α_3	9.5×10^6cm/s
β_1	2.3×10^{-4}cm^3/V^{2}s
β_2	96cm^2/*Vs*
β_3	1.6×10^7cm/s
γ_1	2×10^8cm/s
γ_2	1.2×10^{-5}cm/V
γ_3	1.9×10^7cm/s
E_L	9×10^4V/cm
E_T	2.3×10^5V/cm
E_H	3.3×10^5V/cm
μ	510cm^2/*Vs*
E_C	4.35×10^4V/cm
Z	1 μm
L	0.1 μm
x	0.5
N_D	5×10^{18}/cm^3
d_0	3nm
d_1	50nm
Δd	0.1 nm
T	300K
E_g^{AlN}	6.13 eV
E_g^{GaN}	3.42 eV

relation of electrons in GaN is shown in Fig. 1[23]. The velocity-field curve can be divided into various regions and the mathematical formulation of electron velocity as a function of electric field for each region can be presented as follows [23].

$$\left.\begin{aligned} v &= \mu E/(1+E/E_c) && \text{for region 1, } 0 \le E \le E_L \\ &= \alpha_1 E^2 + \alpha_2 E + \alpha_3 && \text{for region 2, } E_L \le E \le E_T \\ &= \beta_1 E^2 + \beta_2 E + \beta_3 && \text{for region 3, } E_T \le E \le E_H \\ &= \gamma_1 \exp(-\gamma_2 E) + \gamma_3 && \text{for region 4, } E \ge E_H \end{aligned}\right\} \quad \ldots (1)$$

Where, the values of various parameters are presented in Table 1.

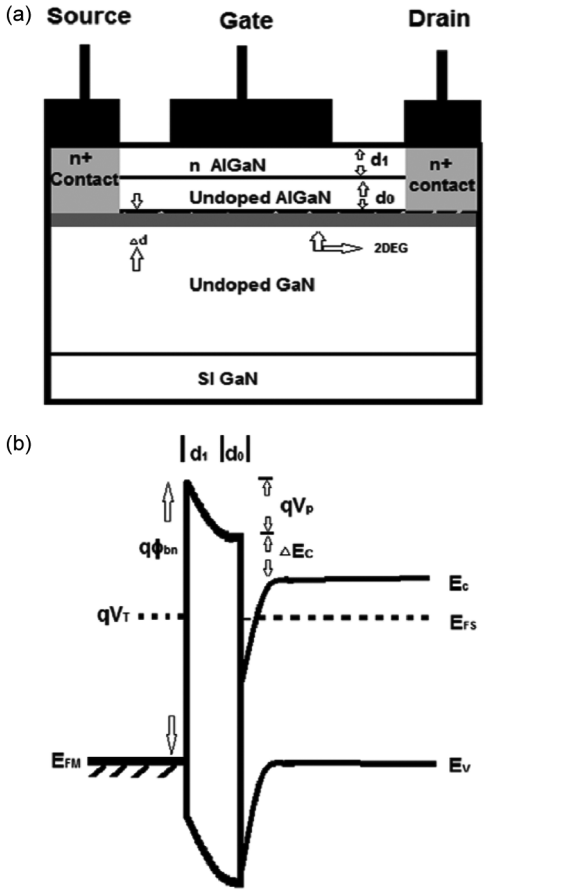

Fig. 2 — (a) A Schematic diagram of GaN MODFET (b) Energy band diagram of gate channel interface.

3 Drain Current

The drain current of a modulation doped field effect transistor is given by [24].

$$\left.\begin{aligned} I &= ZC_i v\left[V_g - V_T - V_y\right] \\ V_T &= \phi_{bn} - \Delta E_c/q - V_P \\ V_p &= qN_d d_1^2/2\varepsilon_s \end{aligned}\right\} \quad \ldots (2)$$

Where, Z is the channel width, C_i is the sheet capacitance, v is the velocity of electrons inside the 2D channel, V_g is the applied gate bias , V_T is the threshold voltage of the device, ϕ_{bn} is the barrier height of the metal-AlGaN junction, ΔE_c is the band gap difference between AlGaN and GaN and V_y is the drain voltage drop at a distance y from the source. Fig. 2(a) shows a schematic diagram of a GaN MODFET having gate length L. The thickness of the doped and undoped AlGaN layer is d_1 and d_0 respectively and Δd is the thickness of the 2D electron gas layer inside GaN. Fig. 2(b) shows the energy band diagram of the gate channel junction of the device.

The analytical forms of the current equations in each field regions are different. The drain current in region 1, region 2, region 3 and region 4 are defined as I_1, I_2, I_3 and I_4 respectively. Using the equations (1) and (2), the drain current of the device in the region 1 of the velocity field curve can be given as

$$I = ZC_i\ \mu E\left[V_g\text{-}V_T\text{-}V_y\right](1+E/E_c)^{-1} \quad \text{... (3)}$$

Where E_c is the critical field of the electron required to attain its peak velocity and E is the source to drain field. Integrating both sides of equation (3) we get,

$$I_1 = Z\mu C_i\left(L+\mu V_D/v_s\right)^{-1}\left[\left(V_g-V_T\right)V_D - V_D^2/2\right] \quad \text{... (4)}$$

Similarly, the drain current of the device for other field regions are calculated as follows

$$I_2 = ZC_i\left[V_g - V_T - V_D/2\right]\left[\alpha_1E^2+\alpha_2E+\alpha_3\right] \quad \text{... (5)}$$

$$I_3 = ZC_i\left[V_g - V_T - V_D/2\right]\left[\beta_1E^2+\beta_2E+\beta_3\right] \quad \text{... (6)}$$

$$I_4 = ZC_i\left[V_g - V_T - V_D/2\right]\left[\gamma_1\exp(-\gamma_2V_D/L)+\gamma_3\right] \quad \text{... (7)}$$

4 Mutual Conductance

The mutual conductance of the device can be derived differentiating drain current with respect to gate voltage. The mutual conductance of the device for various field regions such as G_{m1} for region 1, G_{m2} for region 2, G_{m3} for region 3 and G_{m4} for region 4 are calculated as follows.

$$G_{m1} = Z\mu C_iV_D\left(L+\mu V_D/v_s\right)^{-1} \quad \text{... (8)}$$

$$G_{m2} = ZC_i\left[\alpha_1E^2+\alpha_2E+\alpha_3\right] \quad \text{... (9)}$$

$$G_{m3} = ZC_i\left[\beta_1E^2+\beta_2E+\beta_3\right] \quad \text{... (10)}$$

$$G_{m4} = ZC_i\left[\gamma_1\exp(-\gamma_2V_D/L)+\gamma_3\right] \quad \text{... (11)}$$

5 Drain Conductance

The drain conductance of the device can be calculated differentiating drain current with respect to drain voltage. The drain conductance of the device for various field regions such as G_{d1} for region 1, G_{d2} for region 2, G_{d3} for region 3 and G_{d4} for region 4 are calculated as follows.

$$G_{d1} = (ZC_i\mu/L)\left(V_g - V_D - V_T\right)(1+E/E_c)^{-2} - (\mu EZC_i/2)(1+E/E_c)^{-1} \quad \text{... (12)}$$

$$G_{d2} = (ZC_i/L)\left[2\alpha_1E+\alpha_2\right]\left[V_g - V_T - V_D/2\right] - (ZC_i/2)\left[\alpha_1E^2+\alpha_2E+\alpha_3\right] \quad (13)$$

$$G_{d3} = (ZC_i/L)\left[2\beta_1E+\beta_2\right]\left[V_g - V_T - V_D/2\right] + (ZC_i/2)\left[\beta_1E^2+\beta_2E+\beta_3\right] \quad \text{... (14)}$$

$$G_{d4} = -(ZC_i/2)\left[\gamma_1\exp(-\gamma_2V_D/L)+\gamma_3\right] - (ZC_i/L)\gamma_1\gamma_2\exp(-\gamma_2V_D/L)\left[V_g - V_T - V_D/2\right] \quad \text{... (15)}$$

6 Cut-Off Frequency

The cut-off frequency of the device can be expressed as[24]

$$F_C = G_m/2\pi ZLC_i \quad \text{... (16)}$$

7 Maximum operating Frequency

The maximum operating frequency of a GaN HEMT can be expressed as[7]

$$F_{\max} = 0.5F_c\left[\begin{matrix}\pi F_cC_g\left(R_g+R_s+R_{gs}+2\pi L_s\right)\\ +G_d\left(R_g+R_s+R_{gs}+\pi F_cL_s\right)\end{matrix}\right]^{-0.5} \quad \text{... (17)}$$

Where, R_g, R_s and L_s are the parasitic parameters, R_{gs} is the gate source resistance and can be calculated as follows

$$R_{gs} = L_{gs}/qN_d\mu_{AlGaN}Zd_1 \quad \text{... (17)}$$

8 Data Validation

The functional dependence of drain current as presented in equations (4) to (7), shows its dependence on gate and drain potential and various material and device parameters. In order to cross check the validity of this present model, we compare our result with the experimental data reported earlier[16]. The Fig. 3 shows that our theoretical results based on accurate velocity-field relation of GaN presented in equation (1) matches pretty well with experimental results.

9 DC Characteristics

Figure 4 shows the variation of drain current with drain bias for different gate potential. It is observed

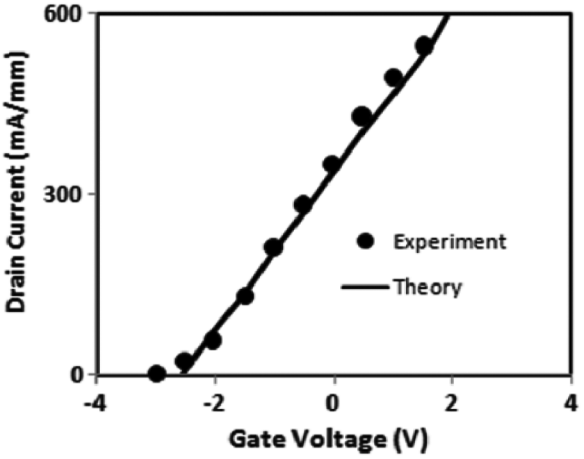

Fig. 3 — Variation of drain current with gate voltage for $V_d = 3V$ and $N_d = 2x10^{18}\ cm^{-2}$.

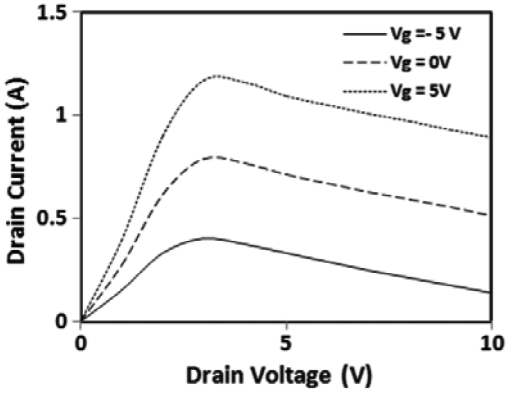

Fig. 4 — Variation of drain current with drain voltage for different gate bias. The material and device parameters taken in calculation are presented in Table 1.

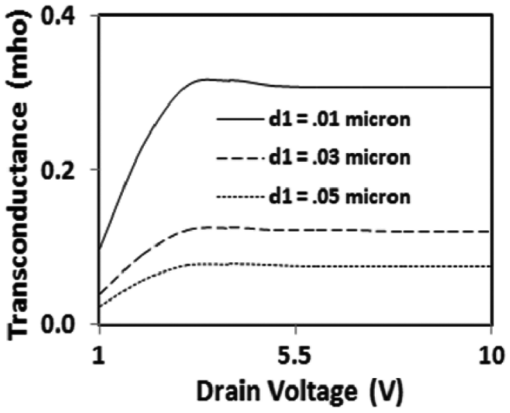

Fig. 5 — Variation of mutual conductance with drain bias for different thickness of doped AlGaN Layer for $V_g = 5V$. The material and device parameters taken in calculation are presented in Table 1.

from the figure that the drain current of the device increases with drain bias for low drain field, achieved a maximum value and for higher drain field the device current reduces. Such nature of variation of drain current with drain bias can be explained from the velocity field curve of GaN. The device characteristics are dependent on velocity of electrons and electron velocity follows the velocity field curve of GaN. It is also observed from figure that the device current increases with gate bias, for positive gate potential the device current is larger and for negative gate bias the device current reduces. This is due to the fact that when the positive potential is applied at the gate terminal, the sheet charge density at the interface of the hetero-junction increases and usually the drain current of the device increases.

The variation of trans-conductance with drain potential for different thickness of doped AlGaN layer is presented in Fig. 5. It is observed from this figure

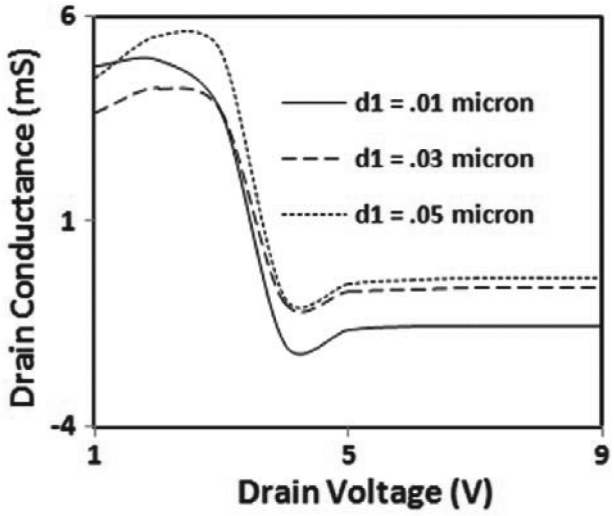

Fig. 6 — Variation of drain conductance with drain potential for different thickness of the doped AlGaN layer for $L = 0.1\mu m$. The other material and device parameters are presented in Table 1.

that the trans-conductance of the device increases initially with drain bias and finally saturates at larger drain potential. Such nature of variation of trans-conductance with drain bias is due to the fact that at lower drain field electron velocity increases with electric field and channel conductivity increases, attains a maximum value and for larger drain field, the conductivity of the channel remains almost unaltered as electron velocity does not change much with drain field. Another important observation is that the conductivity of the channel decreases with thickness (d_1) of the doped AlGaN layer. This is because with the increase of d_1, the sheet capacitance at the gate junction reduces and the electron density inside the 2DEG layer decreases. Thus, the channel becomes more resistive.

The variation of drain conductance with drain voltage is presented in Fig. 6 for different thickness of the doped AlGaN layer. It is observed from the figure that the drain conductance usually increases with the thickness of the doped AlGaN layer. This is because the thick doped layer contributes more number of electrons in 2DEG region and conductivity of the channel is enhanced subsequently. Interestingly, such variation of drain conductivity with d_1 is different from the nature of variation of trans-conductance with d_1 presented in Fig. 5. It is also observed from the figure that the drain conductance of the device decreases with drain bias after a sufficient drain field then tends to increase and finally saturates. Such nature of variation of drain conductance with drain

bias can be explained from velocity field characteristics of GaN. In low field region, the electrons velocity increases with drain bias and drain conductance is maximum. In the subsequent field region, the drain conductance decreases due to negative resistance effect and after a sufficient field the negative resistance effect disappears and the drain conductance of the device saturates.

The variation of threshold voltage of the device with the thickness of the doped AlGaN layer for different values of mole fraction is depicted in Fig. 7. It is very interesting to observe that the threshold voltage of the device changes significantly with the thickness of the doped AlGaN layer. The threshold voltage shifts from positive value to its negative value with the suitable change in d_1. Thus, with the proper selection of d_1 the device can be normally OFF or normally ON. Such nature of variation of threshold voltage is due to the fact that as the d_1 increases, more negative gate potential is required to deplete the doped region and thus threshold voltage becomes negative. On the other hand, for smaller d_1 value, the doped region can be depleted of charge carriers with no gate voltage or positive gate voltage and the threshold voltage becomes positive.

10. RF Characteristics

The RF characteristics of a field effect transistor are very important in order to access its frequency response performance. To study the frequency response of the field effect transistor, we have studied the device cut-off frequency and maximum operating frequency. In Fig. 8, we present the variation of cut-off frequency of the device with drain bias for different values of channel lengths. It is seen from the figure that the cut-off frequency of the device reduces with gate length. The electrons coming from source end have to travel more to reach drain terminal when gate length is longer. At the same time the channel resistance is also enhanced with gate length. These are the limiting factors of cut-off frequency of the device having longer gate length. It is also observed from the figure that the cut-off frequency of the device increases initially for small drain bias and gets constant with larger drain potential. Such variation of cut-off frequency with drain bias can be explained from the relation between electron velocity and electric field. For lower drain field the electron velocity is field dependent and increases with electric field and speed of response of the device is thus enhanced. On the other hand, for larger drain field, the electron velocity *vs*. electric field relation is quite different and change in electron velocity with drain field is smaller compared to its earlier value. As a result of that, the speed of response of the device does not raise much and cut-off frequency of the device becomes constant with drain bias.

The variation of maximum operating frequency with drain bias is presented in Fig. 9 for different channel lengths. This figure shows that the maximum operating frequency of the device usually increases with drain field but for a certain range of drain field it decreases with drain bias. The variation value of maximum operating frequency depends on cut-off frequency and drain conductance of the device over

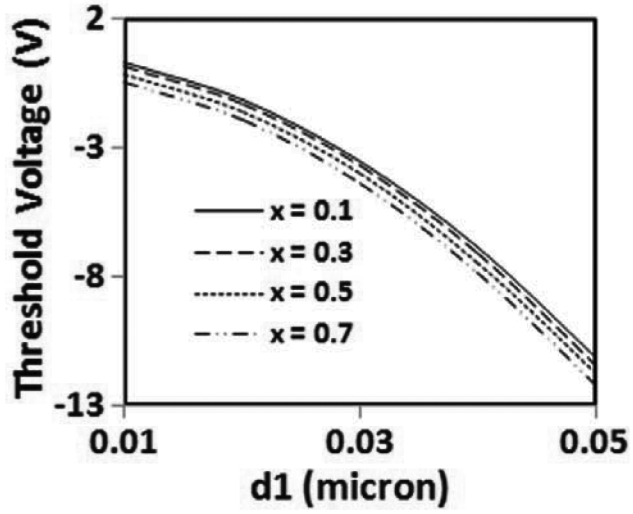

Fig. 7 — Variation of threshold voltage of the device with the thickness of the doped AlGaN layer for different values of mole fraction. The material and device parameters taken in calculation are presented in Table 1.

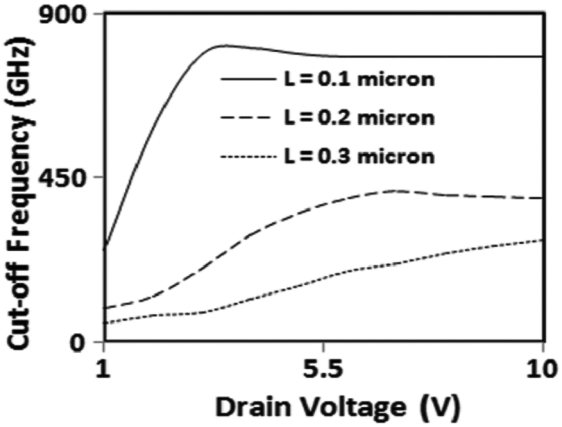

Fig. 8 — Variation of Cut-off frequency with drain voltage for different gate length. The material and device parameters taken in calculation are presented in Table 1.

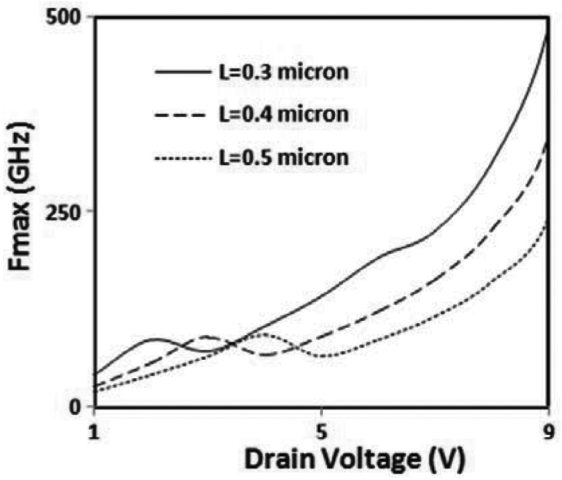

Fig. 9 — Variation of maximum operating frequency with drain voltage for various gate lengths for d_1=.01μm. The other material and device parameters are presented in Table 1.

the entire field region. The reduction of maximum operating frequency with drain bias is due to the negative resistance effect of GaN material in the particular field region. However, the maximum operating frequency of the device decreases with channel length as larger channel requires more time to travel an electron from source to drain.

Conclusions

In conclusion, we have demonstrated the dependence of drain current of a GaN MODFET over the entire field region i.e. from low field to very high field region. The variation of other DC parameters such as drain conductance and mutual conductance are also studied from low field to very high field region. It is observed that the DC parameters of the device depend significantly over the drain field. This work has been extended to study the RF parameters such as cut-off frequency and maximum operating frequency of the device. In addition, the threshold voltage of the device has been studied with respect to mole fraction and thickness of the doped AlGaN layer. The validity of this work is also verified with the experimentally observed data reported earlier.

References

1 Caddemi A, Cardillo E & Crupi G, *Microw Opt Technol Lett*, 58 (2016) 151.
2 Han J, Ferry D K & Newman P, *IEEE Electron Device Lett*, 11 (1990) 209.
3 Alim M A, Rezazadeh A A & Gaquiere C, *Solid-State Electron*, 119 (2016) 11.
4 Dang R, Yang L, Lv Z, Song C & Xu Z, *Electronics*, 8 (2019) 266.
5 Sen S, Pandey M K & Gupta R S, *IEEE Trans Electron Devices*, 46 (1999) 1818.
6 Sen S, Pandey M K, Haldar S & Gupta R S, *J Phys D Appl Phys*, 33 (2000) 18.
7 Kwak H T, Chang S B, Kim H J, Jang K W, Yoon H S, Lee S H, Lim J W & Kim H S, *Appl Sci*, 8 (2018) 974.
8 Palacios T, Dora Y, Chakraborty A, Sanabria C, Keller S, Baars S P D & Mishra U K, *Phys Status Solidi (a)*, 7 (2006) 1845.
9 Li L, Nomoto K, Pan M, Li W, Hickman A, Miller J, Lee K, Hu Z, Bader S J, Lee S M, Hwang J C M, Jena D & Xing H G, *IEEE Electron Device Lett*, 41(2020) 689.
10 Nigam A, Bhat T N, Rajamani S, Dolmanan S B, Tripathy S & Kumar M**,** *AIP Adv*, 7 (2017) 085015.
11 Gryglewski D, Wojtasiak W, Kaminska E & Piotrowska A, *Electronics*, 9 (2020) 1305.
12 Gonschorek M, Carlin, Feltin L E, Py M A & Grandjean N, *J Appl Phys*, 109 (2011) 063720.
13 Sridharan S, Venkatachalam A &Yoder P D, *J Comput Electron*, 7 (2008) 236.
14 Fang Z, *J Phys Conf Ser*, 1699 (2020) 012006.
15 Vitusevich S A, Kurakin A M, Klein N, Petrychuk M V, Naumov A V &. Belyaev A E, *IEEE Trans Device Mater Reliab*, 8 (2008) 543.
16 Rashmi, Haldar S, & Gupta R S, *Microw Opt Technol Lett*, 29 (2001) 117.
17 Rashmi, Agrawal A, Sen S, Haldar S, & Gupta R S, *Microw Opt Technol Lett*, 27 (2000) 413.
18 Cheng X, Li M & Wang Y, *Solid-State Electron*, 54 (2010) 42.
19 Joh J, Gao F, Palacios T & Alamo J A D, *Microelectron Reliab*, 50 (2010) 767.
20 Charfeddine M, Belmabrouk H, Zaidi M A & Maaref H, *J Mod Phys*, 3 (2012) 881.
21 Vitanov S, Palankovski V, Maroldt & Quay R, *Solid-State Electron*, 54 (2010) 1105.
22 Asgari A, Kalafi M & Faraone L, *Phys Stat Sol*, 2 (2005) 1047.
23 Kabra S, Kaur H, Gupta R, Haldar S, Gupta M & Gupta R S, *Microelectron J*, 37 (2006) 620.
24 Sze S M, Semiconductor Devices Physics & Technology, (Wiley-India Publication) 2nd Edn, (2002) 249.